Title
Vps34 regulates Rab7 and late endocytic trafficking through recruitment of the GTPase-activating protein Armus

Journal
Journal of Cell Science, 129(23)

ISSN
0021-9533

Authors
Jaber, Nadia
Mohd-Naim, Noor
Wang, Ziqing
et al.

Publication Date
2016-12-01

DOI
10.1242/jcs.192260

Vps34 regulates Rab7 and late endocytic trafficking through recruitment of the GTPase activating protein Armus

Nadia Jaber[1], Noor Mohd-Naim[2], Ziqing Wang[3], Jennifer L. DeLeon[1], Seong Kim[4], Hua Zhong[5], Namratha Sheshadri[1], Zhixun Dou[1], Aimee L. Edinger[4], Guangwei Du[3], Vania M.M. Braga[2], and Wei-Xing Zong[1,5,6,*]

[1]Department of Molecular Genetics and Microbiology, Stony Brook University, Stony Brook, NY11794, USA

[2]Molecular Medicine, NHLI, Faculty of Medicine, Imperial College London, London SW7 2AZ, UK

[3]Department of Integrative Biology and Pharmacology, University of Texas Health Science Center at Houston, Houston, TX 77030, USA

[4]Department of Developmental and Cell Biology, University of California, Irvine, CA 92697, USA

[5]Department of Chemical Biology, Ernest Mario School of Pharmacy, Rutgers University, 164 Frelinghuysen Road, Piscataway, NJ08854, USA

[6]Rutgers Cancer Institute of New Jersey, 195 Little Albany Street, New Brunswick, NJ08903, USA

*Correspondence to Wei-Xing Zong: weixing.zong@pharmacy.rutgers.edu

Journal of Cell Science • Advance article

JCS Advance Online Article. Posted on 28 October 2016

Summary statement

Vps34 regulates Rab7 and late stages of endocytosis

Abstract

Class III PI 3-kinase Vps34 produces PI(3)P on both early and late endosome membranes to control membrane dynamics. We used Vps34-deficient cells to delineate whether Vps34 has additional roles in endocytic trafficking. In Vps34 knockout mouse embryonic fibroblasts (MEFs), transferrin recycling and EEA1 membrane localization were unaffected despite elevated Rab5-GTP levels. Strikingly, a large increase in Rab7-GTP levels, an accumulation of enlarged late endosomes, and decreased EGFR degradation were observed in Vps34-deficient cells. The hyperactivation of Rab7 in Vps34-deficient cells stemmed from the failure to recruit the Rab7 GAP, Armus, which binds to PI(3)P, to late endosomes. Protein-lipid overlay and liposome binding assays reveal that the putative Pleckstrin homology (PH) domain in Armus can directly bind to PI(3)P. Elevated Rab7-GTP led to the failure of intraluminal vesicle (ILV) formation and lysosomal maturation. Rab7 silencing and Armus overexpression alleviated the vacuolization seen in Vps34-deficient cells. Together, these results demonstrate that Vps34 has a previously unknown role in regulating Rab7 activity and late endosomal trafficking.

Introduction

Vps34 is the sole Class III phosphatidylinositol 3-kinase (PI3K), generating PI(3)P in subcellular locations dictated by its binding partners. When complexed with Vps15, Beclin1, and UVRAG, Vps34 is targeted to early endosomes via the interaction between Vps15 and Rab5 (Christoforidis et al., 1999b). PI(3)P generation by Vps34 at the early endosome recruits effector proteins that contain FYVE or PX domains, such as EEA1, Hrs, Rabenosyn-5 and Rabankyrin-5 (Sato et al., 2001). These effectors regulate the docking and fusion of cargo-containing vesicles from the plasma membrane (Zerial and McBride, 2001), as well as sorting of the enclosed cargo, which can either be recycled back to the plasma membrane or delivered to the lysosome for degradation (Christoforidis et al., 1999a; Huotari and Helenius, 2011; Li et al., 2013; Simonsen et al., 1998).

Endocytic cargo destined for degradation remains in the endosome as it undergoes a maturation process that involves the shedding of Rab5-GTP from the endosome membrane and the simultaneous acquisition of Rab7 (Rink et al., 2005). Active, GTP-bound Rab7 recruits its own set of effectors, including RILP and HOPS, to promote endosome motility and tethering/fusion, respectively (Wang et al., 2011). Fusion of late endosomes with lysosomes facilitates cargo degradation. Intraluminal vesicle (ILV) formation, the inward budding and scission of the endosome membrane, is also an important aspect of endosome maturation (Huotari and Helenius, 2011; Piper and Luzio, 2001). This process both sequesters endocytic cargo from cytosolic proteins and allows for the degradation of membrane proteins within the lysosome. ILV formation is regulated by Hrs, the ESCRT complexes, and PIKfyve, and genetic disruption of these components reduces or prevents ILV formation (Bache et al., 2003; Ikonomov et al., 2003; Saksena et al., 2007). In addition to its role in regulating the early stages of endocytosis, Vps34 has also been implicated in the late stages of endosomal traffic such as ILV formation (Fernandez-Borja et al., 1999; Futter et al., 2001), endosome-lysosome fusion (Luzio et al., 2007; Mullock et al., 1998), and Rab7 interaction (Stein et al., 2003; Vieira et al., 2003).

Rab7 activity is controlled by GTPase activating proteins (GAPs) and guanine nucleotide exchange factors (GEFs). Armus and TBC1D15 act as Rab7 GAPs, while the Mon1-Ccz1 complex acts as a Rab7 GEF (Gerondopoulos et al., 2012; Nordmann et al., 2010; Yasuda et al., 2016). In addition to endocytic trafficking, these regulators play important roles in autophagy:

Armus is a Rac1 effector that interacts with LC3 to regulate Rab7-GTP levels on autophagosomes (Carroll et al., 2013), TBC1D15 interacts with LC3 to regulate Rab7 activity during mitophagy (Yamano et al., 2014), and Mon1-Ccz1 is required for autophagosome-lysosome fusion (Hegedus et al., 2016).

Many of the previous studies on Vps34 function were based on the use of promiscuous PI3K inhibitors like wortmannin, thus the role of Vps34 in the late stage of endocytic trafficking warrants further clarification. Our initial characterization of Vps34 knockout MEFs revealed that early endosome functions were preserved but late endosomal trafficking was severely disrupted (Jaber et al., 2012). Here, we describe an additional role for Vps34 in late endocytic trafficking: Vps34 deletion leads to sustained Rab7 activation due to defective recruitment of its GTPase activating protein (GAP), Armus, to late endosomes. This finding further clarifies the role of mammalian PI3K Vps34 in endocytic trafficking and suggests that PI3P has a more important role at the late endosome than was previously appreciated.

Results

Vps34 functions in autophagy, endocytosis, and mTOR activation are dependent on its catalytic activity

During our characterization of autophagy using MEFs derived from $Vps34^{flox/flox}$ embryos, we observed that Vps34 deletion leads to the formation of enlarged late endosomes, inhibition of EGFR degradation, and inhibition of amino acid-induced mTOR activation (Jaber et al., 2012). Kinase-independent roles have been described for other PI3Ks (Ciraolo et al., 2008; Dou et al., 2013). To determine whether the defects observed in $Vps34^{-/-}$ MEFs are specific consequences of the loss of Vps34 kinase activity, we expressed HA-tagged Vps34 or a kinase-dead (KD) mutant of Vps34, K771A, that fails to interact with the PI substrate (Miller et al., 2010) in $Vps34^{-/-}$ MEFs. Reconstitution with either wild-type or Vps34 KD in the Vps34 knockout MEFs rescued the protein levels of Beclin1, a Vps34 binding partner whose stability is dependent on the formation of the Vps34-Beclin1 complex (Itakura et al., 2008), indicating that the Vps34 KD mutant is capable of forming the complex (Fig. 1A). In contrast, the large increase in the protein level of the negative regulator of autophagy, Rubicon, in Vps34 knockout cells (Devereaux et al., 2013), was corrected by wild-type, but not Vps34 KD (Fig. 1A). This result may reflect the regulation of

Rubicon by autophagic degradation. Consistently, wild-type but not Vps34 KD rescued the block in autophagy flux in Vps34 knockout cells (Fig. 1B). Moreover, Vps34 wild-type but not the KD mutant rescued the vacuolization phenotype (Fig. 1C). In addition, expression of Vps34 wild-type partially rescued EGFR degradation, while the KD mutant failed to do so (Fig. 1D). The abrogated mTOR signaling observed in Vps34 knockout cells, as measured by the phosphorylation of ribosomal protein S6, was also rescued by expression of Vps34 wild-type, but not the KD mutant (Fig. 1E). These data indicate that the defective autophagy, endocytic degradation, and mTOR signaling in Vps34 knockout MEFs are specifically due to Vps34 ablation and these functions are dependent on Vps34 catalytic activity.

Vps34 is dispensable for certain early endocytic events

Vps34 localizes to the early endosome where it helps to recruit effector proteins that contain PI(3)P and Rab5 binding domains, such as EEA1, thereby regulating the delivery and sorting of endocytic cargo (Sato et al., 2001). Surprisingly, we observed no defect in the rate of transferrin recycling in Vps34 knockout cells (Jaber et al., 2012) (Fig. 2A). Consistent with this phenomenon, transferrin colocalized with EEA1 (Fig. 2B), and EEA1 interacted with Rab5 to a similar extent in both wild-type and Vps34 knockout cells (Fig. 2C).

The role of Vps34 in early endosome functions is based mainly on studies using the non-specific PI3K inhibitor wortmannin, which decreases EEA1 membrane localization (Simonsen et al., 1998). To determine if the effects of wortmannin on EEA1 localization are mediated by VPS34 inhibition, we compared EEA1 membrane localization in Vps34 knockout cells and wild-type cells treated with wortmannin. Consistent with previous studies (Chavrier et al., 1991), Rab5 and Rab7 appeared almost exclusively in the membrane fraction (Fig. 2D), although cytoplasmic localization is observed upon longer exposure (data not shown). As expected, wortmannin treatment led to a subtle decrease in EEA1 membrane localization in wild-type cells, similar to what has been previously observed by others (Johnson et al., 2006) (Fig. 2D). However, in Vps34 knockout cells, EEA1 membrane localization was unaffected by wortmannin treatment (Fig. 2D). Immunofluorescence microscopy revealed that endogenous Rab5 and EEA1 colocalized on small punctate structures in untreated wild-type cells, and wortmannin treatment caused the discrete puncta to become disperse and disrupts the colocalization of EEA1 and Rab5 (percent of EEA1

colocalizing with Rab5 was 70.3 with DMSO and 39.1 with wortmannin) (Fig. 2E). Observation by super resolution microscopy (SIM) reveals that EEA1 and Rab5 appear intertwined in untreated wild-type cells. Upon wortmannin treatment, this pattern was disrupted and EEA1 no longer interacted with Rab5 (Fig. 2F). As previously observed, Rab5 and EEA1 co-localized on enlarged endosomes in Vps34-deficient cells (Johnson et al., 2006; Morel et al., 2013), and this localization was unaffected by wortmannin (percent of EEA1 colocalizing with Rab5 was 75.9 with DMSO and 64.2 with wortmannin) (Fig. 2E, F).

Vps34 deficiency leads to hyperactivation of Rab7

In contrast to the relatively intact early endosome functions, Vps34 deletion led to a dramatic block in EGFR degradation (Fig. 1D) (Jaber et al., 2012). Using GFP-tagged EGFR, we observed that after overnight serum starvation, GFP-EGFR localized to the plasma membrane in both wild-type and knockout cells (Fig. 3A). Upon stimulation with EGF, GFP-EGFR accumulated on intracellular puncta in wild-type cells but localized to the limiting membrane of the enlarged membrane structures in knockout cells (Fig.3A). As we and others have characterized the enlarged membrane structures in Vps34-depleted cells as late endosomes, it is likely that the pattern of GFP-EGFR observed in the Vps34 knockout cells represents the limiting membrane of late endosomes. Indeed, immunogold-electron microscopy (EM) against GFP-EGFR confirms that GFP-EGFR is internalized to the lumen of endosomes in wild-type cells, while remaining on the limiting membrane of enlarged membrane structures, presumably endosomes, in the knockout cells (Fig. 3B. In agreement, Alexa Fluor 647-tagged EGF localized to the interior of Rab7- and Lamp1-positive endosomes in wild-type cells, but was restricted to the limiting membrane (visualized as hollow ring-like structures, rather than solid circles) of enlarged Rab7- and Lamp1-positive endosomes in the knockout cells (Fig. 3C). These results corroborate with what others have previously observed with wortmannin treatment (Futter et al., 2001). These data suggest that in the absence of Vps34, EGF and EGFR are not sequestered into ILVs, and instead reside on the limiting membrane of late endosomes.

Rab7 is a small GTPase that regulates membrane fusion reactions at the late endosome, including fusion of late endosomes with lysosomes (Kummel and Ungermann, 2014). During endosome maturation, Rab5-GTP is replaced with Rab7-GTP by a switch mechanism (Rink et al., 2005).

Since we observed defects in late endocytic functions in Vps34 knockout cells, we evaluated the activation state of Rab7 in these cells using a GST-tagged Rab7 binding domain (GST-R7BD) of the Rab7 effector RILP which selectively binds Rab7-GTP (Peralta et al., 2010). Intriguingly, a markedly elevated level of Rab7-GTP was observed in Vps34 knockout cells (Fig. 3D). In wild-type cells, Rab7-GTP levels increased upon serum starvation or EGF stimulation, whereas in Vps34 knockout cells serum starvation and EGF stimulation had no further stimulatory effect (Fig. 3E). To determine whether this hyperactive Rab7 is able to recruit its effectors in Vps34 knockout cells, we expressed GFP-RILP and observed its co-localization with endogenous Rab7. In wild-type cells, as expected, overexpression of GFP-RILP caused clustering of Rab7-positive late endosomes near the microtubule organizing center (Fig. 3F) (Harrison et al., 2003). Imaging with structured illumination microscopy (SIM) revealed the spherical nature of these clustered endosomes (Fig. 3F, right panel). In Vps34 knockout cells, GFP-RILP and Rab7 were also co-localized but were present on the membrane of the swollen late endosomes (Fig. 3F). Therefore, in Vps34-deficient cells, the Rab7-GTP level is drastically increased and is able to recruit its effector RILP. However, despite the elevated Rab7 activity, Vps34 knockout cells were deficient in degradation of endocytic cargo (Fig. 1D). This correlated with the decreased degradative capacity as shown by decreased fluorescence generated by the proteolytic cleavage of DQ-BSA (Fig. 3G), and by the decreased proteolytic cleavage of cathepsin D from the immature (52 kDa) and intermediate (48 kDa) forms into the mature form (33 kDa) in Vps34 knockout cells (Fig. 3H). Together, these data indicate that ablation of Vps34 leads to hyperactivation of Rab7 and the failure of ILV formation and lysosomal maturation.

Rab7 GAP Armus is a PI(3)P binding protein

We next sought to determine how Vps34 regulates Rab7 activity. The activity of small GTPases is modulated by GAPs and guanine nucleotide exchange factors (GEFs) (Fukuda, 2011). Armus has been reported as a Rab7 GAP with a putative PH domain that could mediate PI(3)P binding (Frasa et al., 2010; Lemmon, 2003). Therefore, it is possible that Armus is recruited to PI(3)P-positive structures to promote Rab7-GTP hydrolysis. Indeed, a protein-lipid overlay assay using the PH domain of Armus (GST-Armus-PH) revealed a positive interaction between Armus-PH domain and PI(3)P, as well as PI(4)P, and phosphatidic acid (Fig. 4A). A liposome binding assay further demonstrated that GST-Armus-PH binds to PI(3)P and PI(4)P-containing liposomes, but

not to the control liposome that contains 1,2-dioleoyl-sn-glycero-3-phosphocholine (PC) and 1,2-dioleoyl-sn-glycero-3-phosphoethanolamine (PE), that additionally contains 1,2-dioleoyl-sn-glycero-3-phosphate (PA) (Fig. 4B). Moreover, expression of Armus reduced Rab7-GTP levels in both wild-type and knockout cells (Fig. 4C). Armus subcellular localization can vary between cells but intracellular puncta are present in epithelial cells (Frasa et al., 2010). Due to the lack of reliable antibodies for endogenous proteins, we overexpressed Myc-Armus and Flag-Rab7 in HeLa cells and observed that Armus and Rab7 co-localized (Fig. 4D), similar to Armus and LC3 co-localization as previously reported (Fig. 4D) (Carroll et al., 2013). To determine the role of Vps34 in Armus localization, Vps34 was stably silenced in HeLa cells (Fig. 4E). Similar to Vps34 knockout MEFs, shVps34 HeLa cells acquired a vacuolated morphology representing swollen late endosomes (Fig. 4F). Expression of RFP-Armus in non-targeting control shRNA cells revealed a punctate localization, which was almost completely lost upon Vps34 silencing (Fig. 4G), indicating that Vps34 can regulate the intracellular membrane localization of Armus. In contrast, another Rab7 GAP, TBC1D15, did not significantly alter its subcellular distribution in Vps34-deficient cells (Suppl. Fig. S1).

Overexpression of GFP-2xFYVE can lead to aggregation and sequestration of PI(3)P, thereby displacing other PI(3)P binding proteins (Carpentier et al., 2013). Consistent with the notion that Armus is a PI(3)P binding protein, overexpression of GFP-2xFYVE in wild-type cells displayed a punctate pattern of GFP-2xFYVE and abolished RFP-Armus puncta, whereas in Vps34-silenced cells GFP-2xFYVE displayed a diffused patter indicating the lack of PI(3)P (Fig. 5A). Moreover, intracellular vacuolization due to late endosome swelling has been observed upon inhibition of Vps34 (Jaber et al., 2012; Johnson et al., 2006; Reaves et al., 1996; Ronan et al., 2014). Rab7 activation has been reported to be essential for vacuolization in several conditions such as in yeast and in *Helicobacter pylori* infection (Genisset et al., 2007; Haas et al., 1995; Papini et al., 1997; Schimmoller and Riezman, 1993). Since we observed Rab7 hyperactivation in Vps34 knockout cells, we tested whether the vacuolization in Vps34-deficient cells was due to reduced Armus recruitment and Rab7 hyperactivation. Indeed, silencing Rab7 or ectopic expression of Armus in Vps34 knockout MEFs led to a complete reversal of vacuolization (Fig. 5B-D). Taken together, these data suggest that Vps34 regulates the intracellular localization Rab7 GAP Armus via PI(3)P production to modulate Rab7 activity.

Discussion

Initial work on mammalian phosphatidylinositol 3-kinase Vps34 speculated its major role in endocytic trafficking at the early endosome, recruiting effector proteins along with small GTPase Rab5. However, using cells with genetic ablation of Vps34, we observed no defect in the rate of transferrin recycling (Fig. 2A) and EEA1-Rab5 interaction (Fig. 2B and 2C) in Vps34 knockout cells. These findings suggest two possible scenarios: 1) PI(3)P may be produced by alternative sources such as the Class II PI3Ks (Devereaux et al., 2013; Falasca and Maffucci, 2012; Posor et al., 2013); and/or 2) A compensatory mechanism independent of PI(3)P is triggered to cope with the loss of Vps34. Previous reports indicate that expression of the constitutively active mutant of Rab5 can bypass the loss of EEA1 membrane localization upon wortmannin treatment (Li et al., 2013; Simonsen et al., 1998), and that wortmannin activates Rab5 (Chen and Wang, 2001). In addition, the early endosome proteins EEA1 and Rabenosyn-5 both contain two Rab5 binding domains, suggesting that they could potentially bind two molecules of Rab5-GTP to mediate membrane tethering (Kummel and Ungermann, 2014). While we do not know how Vps34 regulates Rab5 activity, an attractive hypothesis is that Vps34 may recruit the PI(3)P binding protein Mon1, which has been shown to displace the Rab5 GEF Rabex5 to reduce Rab5-GTP (Poteryaev et al., 2010).

We also find that EGF and its receptor accumulate on the limiting membrane of the enlarged late endosomes in Vps34 knockout MEFs, suggesting that the inward budding process of intraluminal vesicle formation is compromised by Vps34 deletion (Fig. 3A-3C). In conjunction with this, we and others have observed that the enlarged late endosomes in Vps34-deficient cells lack internal vesicle structures (Jaber et al., 2012; Johnson et al., 2006). We hypothesize that Vps34 may regulate intraluminal vesicles indirectly. PIKfyve is recruited to $PI(3)P^{+}$ endosomes via its FYVE domain, where it phosphorylates PI(3)P to generate $PI(3,5)P_2$. This phospholipid has been demonstrated to regulate ILV formation and endosome size (Ikonomov et al., 2003; Ikonomov et al., 2015). In addition, ILV formation is also regulated by the ESCRT complexes, and the ESCRT-0 factor (Hrs) is a PI(3)P and Rab5 effector (Bache et al., 2003; Falguieres et al., 2008; Lindmo and Stenmark, 2006). PIKfyve and the ESCRTs may cooperate to regulate ILV formation, as the ESCRT-III subunit Vps24 interacts with $PI(3,5)P_2$ (Lindmo and Stenmark, 2006). Thus, the loss

of Vps34 likely disrupts the normal function of PIKfyve and ESCRTs, which in turn, negatively affects ILV formation.

In contrast to the relatively intact early endosome function, we observe severe defects in late endosome activities such as EGFR degradation, proteolytic activity, and cathepsin D maturation in Vps34 knockout cells (Fig. 1D, 3G, 3H). We also observe a dramatic alteration of late endosome morphology in cells lacking Vps34 (Fig. 1C and 4E), which is consistent with a previous observation of Vps34 knockdown in glioblastoma cells (Johnson et al., 2006). We suspect the defective late endosome function is at least partially caused by abnormal Rab7 activation upon Vps34 ablation, as Rab7-GTP levels are dramatically elevated in Vps34 knockout cells (Fig. 3D and 3E). Interestingly, some previous reports have brought to light a possible role for Vps34 at the late endosome in conjunction with Rab7 (Stein et al., 2003; Vieira et al., 2003). Here we provide evidence that Vps34 regulates Rab7 activity through recruitment of its GAP Armus, which we find is a PI(3)P-binding protein (Fig. 4A and 4B). A similar observation was made in C. elegans where the Armus homolog TBC-2 was found to be a PI3P-binding protein (C. Rocheleau, personal communication). Silencing Vps34 or overexpression of GFP-2xFYVE inhibits the punctate localization of Armus (Fig. 4G and 5A). Under normal conditions, Vps34 may recruit Armus to late endosomes to keep Rab7-GTP levels in check. Given that PI(3)P is present on late endosomes (Cao et al., 2008) and may not be a limiting factor, a second signal may serve to recruit Armus at the precise time to regulate Rab7.

Rab7 regulates the homotypic fusion of late endosomes and the heterotypic fusion of late endosomes with lysosomes (Kummel and Ungermann, 2014). While previous work has established a role for Armus in regulating Rab7 activity during autophagy and mitophagy, we believe our findings support a role for Armus-regulated Rab7 activity in the late endocytic pathway (Carroll et al., 2013; Yamano et al., 2014). Our previous work characterizing the Vps34 knockout MEFs established that the autophaghic pathway is defective in these cells, beginning from the early stages of autophagosome biogenesis (Jaber et al., 2012). Thus, any Rab7 activity in the cells is likely to be associated with other pathways. However, we can't rule out the possibility that a proportion of Rab7 activity may be related to an early step in autophagosome biogenesis.

It is curious that the deletion or knockdown of Vps34 and subsequent increase in Rab7-GTP leads to the same enlarged late endosome phenotype as Rab7 knockdown. Others have observed that expression of both constitutive-active and dominant-negative Rab7 lead to an enlarged late endosome phenotype (Stein et al., 2003). In comparison to the endosomes we observed in Vps34 knockout cells, which do not contain ILVs, enlarged late endosomes in Rab7 knockdown cells were observed to contain increased numbers of ILVs. It was suggested that the late endosomes in Rab7 knockdown cells expand to accommodate the increased number of internal vesicles (Vanlandingham and Ceresa, 2009). Therefore, in the case of Vps34 deletion, while it may lead to the failure of ILV formation via a Rab7-indpendent mechanism, the enlarged late endosomes may be the result of increased homotypic late endosome fusion due to increased Rab7-GTP levels.

We also observed intracellular vacuolization which has also been attributed to Rab7 hyperactivation (Genisset et al., 2007; Haas et al., 1995; Papini et al., 1997; Schimmoller and Riezman, 1993). We were unable to rescue the defects in EGFR degradation and lysosomal function by Rab7 silencing or its dominant-negative mutant (data not shown), possibly due to the requirement of a delicate level of Rab7 activation for these processes. Nonetheless, Rab7 silencing or Armus overexpression suppressed vacuolization in Vps34-deficient cells (Fig. 5B-5D), indicating that at least some of the late endosomal trafficking defects in Vps34-deficient cells can be rescued by Armus-mediated Rab7 inactivation. Given that we believe Armus plays a role in the phenotype of Vps34 knockout cells, we expect that knockdown of Armus would generate a similar phenotype. Unfortunately we were unable to test this hypothesis because shRNA against Armus was not yet available. Moreover, we cannot rule out the possibility that the phenotypes we observe in Vps34 knockout cells are partially due to the loss of $PI(3,5)P_2$, a downstream product of PI(3)P, as $PI(3,5)P_2$-deficient cells have the same vacuolated morphology and $PI(3,5)P_2$ is described to have various roles in late endosome-lysosome fusion (Bonangelino et al., 2002; Dong et al., 2010; Ikonomov et al., 2003). Nonetheless, our work provides evidence of a previously unappreciated role for mammalian Vps34 in the regulation of small GTPase Rab7 and the late stages of endocytic trafficking, and suggests that Vps34 may be suppressed under physiological conditions where intracellular vacuolization was observed such as certain neurodegenerative diseases like Alzheimer's (Chan et al., 2012).

Abbreviations:

EGF, epidermal growth factor; EGFR, epidermal growth factor receptor; ESCRT, endosomal sorting complex required for transport; GAP, GTPase-activating protein; GEF, guanine nucleotide exchange factor; GFP, green fluorescent protein; HOPS, homotypic vacuole fusion and protein sorting complex; LC3, microtubule-associated protein light chain 3; MEF, mouse embryonic fibroblast; mTOR, mammalian target of rapamycin; PE, phosphatidylethanolamine; PH, Pleckstrin homology; PI3K, phosphotinositide 3-kinase; PI, phosphatidyltinositol; PI(3)P, Phosphatidyltinositol 3-phosphate; S6K, p70 S6 kinase; Vps34, vacuolar protein sorting 34.

Materials & Methods

Cells and culture

Vps34$^{flox/flox}$ mouse embryonic fibroblasts (MEFs) were generated as previously described (Jaber et al., 2012). Cells were infected with adenovirus-GFP or adenovirus-Cre-GFP to generate Vps34 wild-type or knockout cells, respectively. Wild-type and knockout cells were made fresh for each experiment. HeLa cells were obtained from ATCC. Both MEFs and HeLa cells were cultured in DMEM supplemented with 10% (vol/vol) FBS (HyClone Fetal Clone III), 100 units per mL penicillin, 100 μg/mL streptomycin and 2 mM glutamine. For starvation assays, MEFs were cultured in serum-free media for 6 h. All cell lines have been tested and authenticated as bacteria and mycoplasma free following ATCC's instructions on a routine basis within 6 month of experiments.

Plasmids

GST-R5BD was described previously (Liu et al., 2007). GST-R7BD, GFP-RILP and GFP-Rab7 plasmids were described previously (Peralta et al., 2010). Rab7 shRNA lentiviral plasmid was purchased from Sigma-Aldrich. Myc-Armus$^{547-928}$, Flag-Armus$^{547-928}$, Myc-Armus$^{1-550}$ and RFP-Armus (full-length) are described elsewhere (Carroll et al., 2013; Frasa et al., 2010). We cloned human Vps34 from a bicistronic Myc-Vps34-V5-Vps15 plasmid (Yan et al., 2009) into the

retroviral LPC vector, and added an HA tag. The Vps34 KD mutant K771A (Miller et al., 2010) was generated by point mutagenesis and was confirmed by PCR.

Antibodies and reagents

We used the following antibodies: Rab5 (D11, Santa Cruz Biotechnology, 1:300 for IF; Cell Signaling Technology, 1:5,000 for WB), EEA1 (Cell Signaling Technology #2411, 1:5,000 for WB; 1:400 for IF), Vps34 (Cell Signaling Technology #4263, 1:1,000 for WB), Hrs (Alexis-Enzo Life Sciences, 1:3,000 for WB), Rab7 (Cell Signaling Technology #9367, 1:5,000 for WB; 1:300 for IF), tubulin (Sigma-Aldrich T4026, 1:10,000 for WB), Ras (Invitrogen, 1:10,000 for WB), Flag (M2, Sigma-Aldrich, 1:1,000 for WB), lamin (M-20, Santa Cruz Biotechnology, 1:500 for WB), EGFR (Abcam AB40815, 1:500 for WB), cathepsin D (C-20, Santa Cruz Biotechnology, 1:250), and LAMP1 (Developmental Studies Hybridoma Bank H4A3, 1:300 for IF). Alexa-Fluor secondary antibodies (1:500) were purchased from Life Technologies. DMEM was purchased from Invitrogen, E64D (10 μg/mL) from EMD, wortmannin (1.0 or 0.1 μM) from EMD Millipore, Transferrin-Alexa Fluor-594 (1.5 μg/mL) from Life Technologies, Ponceau from Sigma-Aldrich, DQ Red BSA (10 μg/mL) from Life Technologies, Dextran Oregon Green MW 10,000 (10 μg/mL) from Molecular Probes, DAPI (4',6'-diamidino-2-phenylindole; 1 μg/ml) from Sigma, Prote-CEASE-M (1:100) from GBiosciences, and Pierce BCA Protein Assay from Thermo Scientific.

Immunofluorescence

Cells were plated at 3–5 × 10^4 cells per well on gelatin-coated glass coverslips in 24-well plates. After treatment, cells were fixed in 4% (wt/vol) paraformaldehyde (PFA) in PBS for 20 min at room temperature. Cells were washed twice with PBS and permeabilized with 0.1% Triton X-100 in PBS for 10 min. Cells were washed three times with PBS and blocked in 5% (wt/vol) goat serum in PBS for 1 h. Primary antibodies were added in 5% (wt/vol) BSA in PBS plus 0.1% Tween-20 (PBST) overnight at 4°C. Cells were washed four times with PBS. Fluorophore-conjugated secondary antibodies were added (1:500) in 5% BSA in PBST for 1 h at room temperature with gentle shaking. Cells were washed three times with PBST, twice with PBS, and then mounted with Immuno-Mount.

Immunoprecipitation

Cells were lysed in general lysis buffer (30 mM Tris [pH 7.5], 150 mM NaCl, 10% glycerol, 1% Triton X-100) plus protease inhibitor cocktail (1:100) and phenylmethylsulfonyl fluoride (PMSF, 200 μM) on ice for 20 minutes with frequent vortexing. Lysates were cleared by centrifuging at 14,000 xg for 10 min at 4°C. After protein quantitation 4 μg IgG or 2 μg Rab5 antibody (D-11, Santa Cruz Biotechnology) were added to lysates and incubated on a rotator at 4°C overnight. The following day, equal volumes of protein G and A (Roche) were aliquoted and washed with general lysis buffer four times. Washed beads were added to the lysates and incubated on a rotator at 4°C for 4 h. The precipitates were washed six times with general lysis buffer, before displacing the precipitated proteins with SDS loading dye.

Immunogold-EM

Vps34 WT or KO MEFs transfected with GFP-EGFR were starved overnight, then left untreated or stimulated with 100 ng/mL EGF in serum-free media for 1.5 h. Cells were fixed for 1 h in cold 4% PFA plus 0.1% glutaraldehyde in PBS at room temperature, then washed three times with PBS, 5 min each. Cells were permeabilized and blocked in 0.2% saponin, 10% BSA, 10% goat serum in PBS for 30 min at room temperature, then washed once with PBS for 5 min. Cells were incubated with anti-rabbit-GFP antibody in 10% BSA (PBS) overnight at 4°C. Cells were washed six times with PBS, 10 min each. Cells were incubated with anti-rabbit antibody conjugated to 1.4-nm gold in 10% BSA (PBS) for 2 h. Cells were washed six times with PBS, 10 min each. Cells were post-fixed with 1% glutaraldehyde in PBS for 10 min, then washed three times with 50 mM glycine in PBS, 5 min each. Cells were then washed three times with 1% BSA in PBS, and three times with distilled water, 5 min each. Cells were incubated with Gold enhance EM Plus (Nanoprobes) for 3-5 min, then rinse with distilled water. The samples were then processed with standard procedure, as previously described (Dou et al., 2010).

Transfection, retroviral and lentiviral infection

MEFs were transfected with Lipofectamine 2000 (Invitrogen) or TransIT X2 (Mirus) 2-3 days following adenoviral infection, following manufacturer's protocol that is optimized for MEFs.

For retroviral or lentiviral infections 293T cells were transfected with the experimental plasmid, ΔR8.91 and VSV-G with Lipofectamine 2000 (Invitrogen). Virus-containing supernatant was

collected at 24, 48 and 72 h post-transfection. Filtered virus-containing supernatant was added to Vps34$^{flox/flox}$ MEFs in suspension for 5 min before plating the cells. Fresh aliquots of virus were added to the cells every 8 to 12 h. Following a 24 h recovery, the cells were selected with 2 μg/mL puromycin for 2 to 3 days or until uninfected control cells were dead.

Transferrin internalization

For transferrin internalization assays, cells were serum starved for 4 h, loaded with 1.5 μg/mL Alexa Fluor-594 conjugated transferrin (Life Technologies) at 4 °C for 40 min, and then incubated for 2 or 5 min at 37 °C. At the end of each time point, cells were subjected to acid wash (10 mM acetic acid and 150 mM NaCl, pH 3.5) for 5 min at 4 °C, and then fixed with 4% paraformaldehyde. Immunofluorescence for EEA1 was then performed.

GST-R7BD pulldown

The preparation of GST-R7BD linked to glutathione agarose beads has been described elsewhere (Peralta et al., 2010). We followed the published protocol with slight modifications. Glutathione agarose beads (Invitrogen) were washed twice with wash buffer (30 mM Tris [pH 7.5], 150 mM NaCl, 10% glycerol, 1% Triton X-100, 10 mM NaF, 100 μM orthovanadate, 200 μM phenylmethylsulfonyl fluoride [PMSF]). Glutathione agarose beads were incubated with GST-R7BD-expressing bacterial lysates for 2-3 h at 4 °C on a rotator. The beads were washed four times, 10 minutes each, with wash buffer at 4 °C on a rotator. Cells were lysed in Rab7 buffer (20mM HEPES, 100 mM NaCl, 5mM MgCl2, 1% triton x-100; plus PMSF (200 μM) and Prote-CEASE-M (1:100). Lysates were cleared by centrifuging at 14,000 x g at 4 °C. After protein quantitation equal amounts of protein were added to the washed GST-R7BD beads and incubated at 4 °C on a rotator overnight. The beads were washed with Rab7 buffer plus DTT (1 μM) 4 times, 5 min each. After the final wash the samples were boiled in 1x SDS loading dye.

DQ-BSA assay

Cells were plated on 30 mm glass-bottomed dishes (MatTek). After overnight recovery cells were loaded with 0.5 mg/mL Dextran-Oregon Green for 16 h plus 4 h chase, then loaded with 10 μg/mL DQ-BSA for 1 h. Cells were washed 3 times with PBS, then incubated in fresh media for 30 min. Live cells were imaged by taking pictures of 5-10 randomly chosen areas.

EGF transport and EGFR degradation assays

For EGF transport, cells were serum starved overnight then stimulated with 100 ng/mL EGF-Alexa Fluor-647 (Life Technologies) in cold serum-free media for 1 h at 4 °C. Cells were then incubated in pre-warmed serum-free DMEM at 10 or 45 min before fixing with 4% paraformaldehyde and performing immunofluorescence. For EGFR degradation, cells were serum-starved overnight then stimulated with 100 ng/mL EGF in serum-free medium for the indicated time points. Cells were rinsed twice with PBS and lysed in RIPA buffer plus 1% SDS, protease inhibitor cocktail (1:100) and EDTA (5 mM).

Protein-lipid overlay assay

PIP strips (Echelon Biosciences, Utah, USA) spotted with 15 different lipids were blocked with blocking buffer (phosphate-buffered saline (PBS), 0.1% Tween-20, 3% fatty-acid free BSA (PBS-T 3% BSA)) and gently agitated overnight at 4 °C. GST-Armus$^{31\text{-}147}$ was incubated with the membrane at a concentration of 0.5 μg/ml in PBS-T 3% BSA for 1 h at room temperature with gentle agitation. 0.5 μg/ml of GST only was used as a negative control and 0.5 μg/ml of PLC-δ1-PH-GST (provided with PIP strip when purchased) as a positive control. Bound protein on lipids was detected using mouse anti-GST antibody in PBS-T 3% BSA followed by HRP-coupled anti-mouse IgG in PBS-T 3% BSA, both for 1 h at room temperature with gentle agitation. Membranes were washed three times for 5 min in PBST in between incubations with protein and antibodies. Positive binding on membranes were visualized with ECL detection kit (GE Healthcare) and exposed to Hyperfilm ECL (GE Healthcare).

Liposome pulldown assay

Liposomes were prepared as described previously (Roach et al., 2012; Zhang et al., 2014). 1,2-dioleoyl-sn-glycero-3-phosphocholine (PC), 1,2-dioleoyl-sn-glycero-3-phosphoethanolamine (PE), 1,2-dioleoyl-sn-glycero-3-phosphate (PA), 1,2-dioleoyl-sn-glycero-3-phospho-(1'-myo-inositol-3'-phosphate) (PI3P) and 1,2-dioleoyl-sn-glycero-3-phospho-(1'-myo-inositol-4'-phosphate) (PI4P) were from Avanti Polar Lipids (Alabaster, AL). In brief, the control liposomes were prepared by mixing PC and PE at a molar ratio of 67:33. Liposomes containing acidic phospholipids were prepared by mixing PC, PE, and PA, PI3P or PI4P at a molar ratio of 65:32:3.

After dried by a rotatory vacuum, the lipid mixtures were re-suspended with the insider buffer (256 mM sucrose, 20 mM Tris-HCl, pH 7.4), and subjected to 10 cycles of freezing in liquid nitrogen and thawing in 37°C water bath. The formed multilamellar lipids were then extruded through polycarbonate membranes (pore size 100 nm, Whatman) for 10 times to generate small unilamellar liposomes. After washed with the binding buffer (150 mM NaCl, 20 mM Tris-HCl pH7.4) and centrifuged at 30,000 x g for 1 h, the pelleted liposomes were re-suspended with the binding buffer and used within 1 week. 10 pmol purified GST or GST-Armus-PH protein was mixed and incubated with the serially diluted liposomes at 4°C for 30 min. After centrifuge at 30,000 x g for 30 min, the supernatants were carefully removed. The pellets were resuspended with 1 x SDS loading buffer and boiled for 5 min, and then separated by SDS-PAGE. The binding of GST-Armus-PH to liposomes was detected by an anti-GST antibody (Abcam) and followed by an IRDye 680-conjugated secondary antibody (Rockland Immunochemicals, Gilbertsville, PA), and visualized by a LI-COR Odyssey imaging system. Quantification of the intensity of Western results was done using ImageJ.

Statistics

Student's t-test was used to compare the differences between two groups. Significance was judged when $p<0.05$. Average plus standard deviation (S.D.) are shown. When sample size (n) was small ($n = 3$ or 4), Kolmogorov–Smirnov (K-S) test was used to check the normality of the data and to ensure the validity of the t-tests.

Image processing and densitometry measurement

Fluorescence and immunofluorescence was analyzed by Zeiss Deconvolution Microscope with AxioCam HRM (Zeiss), Zeiss LSM 510 META NLO Laser Scanning Confocal Microscope system, or Nikon N-SIM super Resolution Microscope system with EMCCD camera iXon3 DU-897E (Andor Technology Ltd.). Images taken from deconvolution and confocal microscopes were viewed and processed by AxioVision LE and Zeiss LSM image browser, respectively. Images were processed in Adobe Photoshop to enhance the brightness and contrast. Densitometry of immunoblot bands was determined by ImageJ software. Background was subtracted from respective measurements for the protein of interest and loading control. Values are expressed as measurement for protein of interest divided by loading control. Colocalization was assessed by

using Image J (https://imagej.nih.gov/ij/download.html) and JACoP v2.0 plugin (http://imagejdocu.tudor.lu/doku.php?id=plugin:analysis:jacop_2.0:just_another_colocalization_plugin:start).

Acknowledgements

We thank Drs. Deborah Brown, Kevin Czaplinski, Michael Frohman, Richard Lin (Stony Brook University, New York, U.S.A.), Christian Rocheleau (McGill University, Quebec, Canada), and Zhenyu Yue (Mount Sinai School of Medicine, New York, U.S.A.) for reagents and suggestions. We thank Guowei Tian and Susan Van Horn (Stony Brook Microscopy Imaging Center, New York, U.S.A.) for assistance on fluorescence and SIM microscopy and electron microscopy, respectively, and Dr. Song Wu (Stony Brook University) for assistance on statistical analysis.

Competing interest

None

Author contributions

NJ and WXZ conceived the ideas, designed the experiments, and wrote the paper. NMN and VMMB performed the PIP strip binding assay. ZW and GD performed the liposome assay. JLD, HZ, NS, and ZD helped with Rab7 activation, subcellular localization, and EGFR turnover assays. SK and ALE performed helped with the TBC1D15 assay and provided critical reagents. All authors performed data analysis of respective experiments.

Funding:

This work is supported by NIH (R01GM97355 and R01CA129536 to W.X.Z., R01HL119478 to G.D., and the Ruth L. Kirschstein National Research Service Award F31CA177243 to N.J.).

References

Bache, K.G., A. Brech, A. Mehlum, and H. Stenmark. 2003. Hrs regulates multivesicular body formation via ESCRT recruitment to endosomes. *J Cell Biol*. 162:435-442.

Bonangelino, C.J., J.J. Nau, J.E. Duex, M. Brinkman, A.E. Wurmser, J.D. Gary, S.D. Emr, and L.S. Weisman. 2002. Osmotic stress-induced increase of phosphatidylinositol 3,5-bisphosphate requires Vac14p, an activator of the lipid kinase Fab1p. *J Cell Biol*. 156:1015-1028.

Cao, C., J.M. Backer, J. Laporte, E.J. Bedrick, and A. Wandinger-Ness. 2008. Sequential actions of myotubularin lipid phosphatases regulate endosomal PI(3)P and growth factor receptor trafficking. *Mol Biol Cell*. 19:3334-3346.

Carpentier, S., F. N'Kuli, G. Grieco, P. Van Der Smissen, V. Janssens, H. Emonard, B. Bilanges, B. Vanhaesebroeck, H.P. Gaide Chevronnay, C.E. Pierreux, D. Tyteca, and P.J. Courtoy. 2013. Class III phosphoinositide 3-kinase/VPS34 and dynamin are critical for apical endocytic recycling. *Traffic*. 14:933-948.

Carroll, B., N. Mohd-Naim, F. Maximiano, M.A. Frasa, J. McCormack, M. Finelli, S.B. Thoresen, L. Perdios, R. Daigaku, R.E. Francis, C. Futter, I. Dikic, and V.M. Braga. 2013. The TBC/RabGAP Armus coordinates Rac1 and Rab7 functions during autophagy. *Dev Cell*. 25:15-28.

Chan, R.B., T.G. Oliveira, E.P. Cortes, L.S. Honig, K.E. Duff, S.A. Small, M.R. Wenk, G. Shui, and G. Di Paolo. 2012. Comparative lipidomic analysis of mouse and human brain with Alzheimer disease. *J Biol Chem*. 287:2678-2688.

Chavrier, P., J.P. Gorvel, E. Stelzer, K. Simons, J. Gruenberg, and M. Zerial. 1991. Hypervariable C-terminal domain of rab proteins acts as a targeting signal. *Nature*. 353:769-772.

Chen, X., and Z. Wang. 2001. Regulation of epidermal growth factor receptor endocytosis by wortmannin through activation of Rab5 rather than inhibition of phosphatidylinositol 3-kinase. *EMBO Rep*. 2:842-849.

Christoforidis, S., H.M. McBride, R.D. Burgoyne, and M. Zerial. 1999a. The Rab5 effector EEA1 is a core component of endosome docking. *Nature*. 397:621-625.

Christoforidis, S., M. Miaczynska, K. Ashman, M. Wilm, L. Zhao, S.C. Yip, M.D. Waterfield, J.M. Backer, and M. Zerial. 1999b. Phosphatidylinositol-3-OH kinases are Rab5 effectors. *Nat Cell Biol*. 1:249-252.

Ciraolo, E., M. Iezzi, R. Marone, S. Marengo, C. Curcio, C. Costa, O. Azzolino, C. Gonella, C. Rubinetto, H. Wu, W. Dastru, E.L. Martin, L. Silengo, F. Altruda, E. Turco, L. Lanzetti, P. Musiani, T. Ruckle, C. Rommel, J.M. Backer, G. Forni, M.P. Wymann, and E. Hirsch. 2008. Phosphoinositide 3-kinase p110beta activity: key role in metabolism and mammary gland cancer but not development. *Sci Signal*. 1:ra3.

Devereaux, K., C. Dall'Armi, A. Alcazar-Roman, Y. Ogasawara, X. Zhou, F. Wang, A. Yamamoto, P. De Camilli, and G. Di Paolo. 2013. Regulation of mammalian autophagy by class II and III PI 3-kinases through PI3P synthesis. *PLoS One*. 8:e76405.

Dong, X.P., D. Shen, X. Wang, T. Dawson, X. Li, Q. Zhang, X. Cheng, Y. Zhang, L.S. Weisman, M. Delling, and H. Xu. 2010. PI(3,5)P(2) controls membrane trafficking by direct activation of mucolipin Ca(2+) release channels in the endolysosome. *Nature communications*. 1:38.

Dou, Z., M. Chattopadhyay, J.A. Pan, J.L. Guerriero, Y.P. Jiang, L.M. Ballou, Z. Yue, R.Z. Lin, and W.X. Zong. 2010. The class IA phosphatidylinositol 3-kinase p110-{beta} subunit is a positive regulator of autophagy. *J Cell Biol*. 191:827-843.

Dou, Z., J.A. Pan, H.A. Dbouk, L.M. Ballou, J.L. DeLeon, Y. Fan, J.S. Chen, Z. Liang, G. Li, J.M. Backer, R.Z. Lin, and W.X. Zong. 2013. Class IA PI3K p110beta subunit promotes autophagy through Rab5 small GTPase in response to growth factor limitation. *Mol Cell*. 50:29-42.

Falasca, M., and T. Maffucci. 2012. Regulation and cellular functions of class II phosphoinositide 3-kinases. *Biochem J*. 443:587-601.

Falguieres, T., P.P. Luyet, C. Bissig, C.C. Scott, M.C. Velluz, and J. Gruenberg. 2008. In vitro budding of intralumenal vesicles into late endosomes is regulated by Alix and Tsg101. *Molecular biology of the cell*. 19:4942-4955.

Fernandez-Borja, M., R. Wubbolts, J. Calafat, H. Janssen, N. Divecha, S. Dusseljee, and J. Neefjes. 1999. Multivesicular body morphogenesis requires phosphatidyl-inositol 3-kinase activity. *Curr Biol*. 9:55-58.

Frasa, M.A., F.C. Maximiano, K. Smolarczyk, R.E. Francis, M.E. Betson, E. Lozano, J. Goldenring, M.C. Seabra, A. Rak, M.R. Ahmadian, and V.M. Braga. 2010. Armus is a Rac1 effector that inactivates Rab7 and regulates E-cadherin degradation. *Curr Biol*. 20:198-208.

Fukuda, M. 2011. TBC proteins: GAPs for mammalian small GTPase Rab? *Bioscience reports*. 31:159-168.

Futter, C.E., L.M. Collinson, J.M. Backer, and C.R. Hopkins. 2001. Human VPS34 is required for internal vesicle formation within multivesicular endosomes. *The Journal of cell biology*. 155:1251-1264.

Genisset, C., A. Puhar, F. Calore, M. de Bernard, P. Dell'Antone, and C. Montecucco. 2007. The concerted action of the Helicobacter pylori cytotoxin VacA and of the v-ATPase proton pump induces swelling of isolated endosomes. *Cellular microbiology*. 9:1481-1490.

Gerondopoulos, A., L. Langemeyer, J.R. Liang, A. Linford, and F.A. Barr. 2012. BLOC-3 mutated in Hermansky-Pudlak syndrome is a Rab32/38 guanine nucleotide exchange factor. *Current biology : CB*. 22:2135-2139.

Haas, A., D. Scheglmann, T. Lazar, D. Gallwitz, and W. Wickner. 1995. The GTPase Ypt7p of Saccharomyces cerevisiae is required on both partner vacuoles for the homotypic fusion step of vacuole inheritance. *EMBO J*. 14:5258-5270.

Harrison, R.E., C. Bucci, O.V. Vieira, T.A. Schroer, and S. Grinstein. 2003. Phagosomes fuse with late endosomes and/or lysosomes by extension of membrane protrusions along microtubules: role of Rab7 and RILP. *Mol Cell Biol*. 23:6494-6506.

Hegedus, K., S. Takats, A. Boda, A. Jipa, P. Nagy, K. Varga, A.L. Kovacs, and G. Juhasz. 2016. The Ccz1-Mon1-Rab7 module and Rab5 control distinct steps of autophagy. *Molecular biology of the cell*.

Huotari, J., and A. Helenius. 2011. Endosome maturation. *EMBO J*. 30:3481-3500.

Ikonomov, O.C., D. Sbrissa, M. Foti, J.L. Carpentier, and A. Shisheva. 2003. PIKfyve controls fluid phase endocytosis but not recycling/degradation of endocytosed receptors or sorting of procathepsin D by regulating multivesicular body morphogenesis. *Mol Biol Cell*. 14:4581-4591.

Ikonomov, O.C., D. Sbrissa, M. Venkatareddy, E. Tisdale, P. Garg, and A. Shisheva. 2015. Class III PI 3-kinase is the main source of PtdIns3P substrate and membrane recruitment signal for PIKfyve constitutive function in podocyte endomembrane homeostasis. *Biochimica et biophysica acta*. 1853:1240-1250.

Itakura, E., C. Kishi, K. Inoue, and N. Mizushima. 2008. Beclin 1 forms two distinct phosphatidylinositol 3-kinase complexes with mammalian Atg14 and UVRAG. *Mol Biol Cell*. 19:5360-5372.

Jaber, N., Z. Dou, J.S. Chen, J. Catanzaro, Y.P. Jiang, L.M. Ballou, E. Selinger, X. Ouyang, R.Z. Lin, J. Zhang, and W.X. Zong. 2012. Class III PI3K Vps34 plays an essential role in autophagy and in heart and liver function. *Proc Natl Acad Sci U S A*. 109:2003-2008.

Johnson, E.E., J.H. Overmeyer, W.T. Gunning, and W.A. Maltese. 2006. Gene silencing reveals a specific function of hVps34 phosphatidylinositol 3-kinase in late versus early endosomes. *J Cell Sci*. 119:1219-1232.

Kummel, D., and C. Ungermann. 2014. Principles of membrane tethering and fusion in endosome and lysosome biogenesis. *Curr Opin Cell Biol*. 29:61-66.

Lemmon, M.A. 2003. Phosphoinositide recognition domains. *Traffic*. 4:201-213.

Li, X., A.G. Garrity, and H. Xu. 2013. Regulation of membrane trafficking by signalling on endosomal and lysosomal membranes. *J Physiol*. 591:4389-4401.

Lindmo, K., and H. Stenmark. 2006. Regulation of membrane traffic by phosphoinositide 3-kinases. *Journal of cell science*. 119:605-614.

Liu, J., D. Lamb, M.M. Chou, Y.J. Liu, and G. Li. 2007. Nerve growth factor-mediated neurite outgrowth via regulation of Rab5. *Mol Biol Cell*. 18:1375-1384.

Luzio, J.P., N.A. Bright, and P.R. Pryor. 2007. The role of calcium and other ions in sorting and delivery in the late endocytic pathway. *Biochem Soc Trans*. 35:1088-1091.

Miller, S., B. Tavshanjian, A. Oleksy, O. Perisic, B.T. Houseman, K.M. Shokat, and R.L. Williams. 2010. Shaping development of autophagy inhibitors with the structure of the lipid kinase Vps34. *Science*. 327:1638-1642.

Morel, E., Z. Chamoun, Z.M. Lasiecka, R.B. Chan, R.L. Williamson, C. Vetanovetz, C. Dall'Armi, S. Simoes, K.S. Point Du Jour, B.D. McCabe, S.A. Small, and G. Di Paolo. 2013. Phosphatidylinositol-3-phosphate regulates sorting and processing of amyloid precursor protein through the endosomal system. *Nature communications*. 4:2250.

Mullock, B.M., N.A. Bright, C.W. Fearon, S.R. Gray, and J.P. Luzio. 1998. Fusion of lysosomes with late endosomes produces a hybrid organelle of intermediate density and is NSF dependent. *J Cell Biol*. 140:591-601.

Nordmann, M., M. Cabrera, A. Perz, C. Brocker, C. Ostrowicz, S. Engelbrecht-Vandre, and C. Ungermann. 2010. The Mon1-Ccz1 complex is the GEF of the late endosomal Rab7 homolog Ypt7. *Current biology : CB*. 20:1654-1659.

Papini, E., B. Satin, C. Bucci, M. de Bernard, J.L. Telford, R. Manetti, R. Rappuoli, M. Zerial, and C. Montecucco. 1997. The small GTP binding protein rab7 is essential for cellular vacuolation induced by Helicobacter pylori cytotoxin. *EMBO J*. 16:15-24.

Peralta, E.R., B.C. Martin, and A.L. Edinger. 2010. Differential effects of TBC1D15 and mammalian Vps39 on Rab7 activation state, lysosomal morphology, and growth factor dependence. *J Biol Chem*. 285:16814-16821.

Piper, R.C., and J.P. Luzio. 2001. Late endosomes: sorting and partitioning in multivesicular bodies. *Traffic*. 2:612-621.

Posor, Y., M. Eichhorn-Gruenig, D. Puchkov, J. Schoneberg, A. Ullrich, A. Lampe, R. Muller, S. Zarbakhsh, F. Gulluni, E. Hirsch, M. Krauss, C. Schultz, J. Schmoranzer, F. Noe, and V. Haucke. 2013. Spatiotemporal control of endocytosis by phosphatidylinositol-3,4-bisphosphate. *Nature*. 499:233-237.

Poteryaev, D., S. Datta, K. Ackema, M. Zerial, and A. Spang. 2010. Identification of the switch in early-to-late endosome transition. *Cell*. 141:497-508.

Reaves, B.J., N.A. Bright, B.M. Mullock, and J.P. Luzio. 1996. The effect of wortmannin on the localisation of lysosomal type I integral membrane glycoproteins suggests a role for phosphoinositide 3-kinase activity in regulating membrane traffic late in the endocytic pathway. *J Cell Sci*. 109 (Pt 4):749-762.

Rink, J., E. Ghigo, Y. Kalaidzidis, and M. Zerial. 2005. Rab conversion as a mechanism of progression from early to late endosomes. *Cell*. 122:735-749.

Roach, A.N., Z. Wang, P. Wu, F. Zhang, R.B. Chan, Y. Yonekubo, G. Di Paolo, A.A. Gorfe, and G. Du. 2012. Phosphatidic acid regulation of PIPKI is critical for actin cytoskeletal reorganization. *Journal of lipid research*. 53:2598-2609.

Ronan, B., O. Flamand, L. Vescovi, C. Dureuil, L. Durand, F. Fassy, M.F. Bachelot, A. Lamberton, M. Mathieu, T. Bertrand, J.P. Marquette, Y. El-Ahmad, B. Filoche-Romme, L. Schio, C. Garcia-Echeverria, H. Goulaouic, and B. Pasquier. 2014. A highly potent and selective Vps34 inhibitor alters vesicle trafficking and autophagy. *Nature chemical biology*. 10:1013-1019.

Saksena, S., J. Sun, T. Chu, and S.D. Emr. 2007. ESCRTing proteins in the endocytic pathway. *Trends Biochem Sci*. 32:561-573.

Sato, T.K., M. Overduin, and S.D. Emr. 2001. Location, location, location: membrane targeting directed by PX domains. *Science*. 294:1881-1885.

Schimmoller, F., and H. Riezman. 1993. Involvement of Ypt7p, a small GTPase, in traffic from late endosome to the vacuole in yeast. *J Cell Sci*. 106 (Pt 3):823-830.

Simonsen, A., R. Lippe, S. Christoforidis, J.M. Gaullier, A. Brech, J. Callaghan, B.H. Toh, C. Murphy, M. Zerial, and H. Stenmark. 1998. EEA1 links PI(3)K function to Rab5 regulation of endosome fusion. *Nature*. 394:494-498.

Stein, M.P., Y. Feng, K.L. Cooper, A.M. Welford, and A. Wandinger-Ness. 2003. Human VPS34 and p150 are Rab7 interacting partners. *Traffic*. 4:754-771.

Vanlandingham, P.A., and B.P. Ceresa. 2009. Rab7 regulates late endocytic trafficking downstream of multivesicular body biogenesis and cargo sequestration. *The Journal of biological chemistry*. 284:12110-12124.

Vieira, O.V., C. Bucci, R.E. Harrison, W.S. Trimble, L. Lanzetti, J. Gruenberg, A.D. Schreiber, P.D. Stahl, and S. Grinstein. 2003. Modulation of Rab5 and Rab7 recruitment to phagosomes by phosphatidylinositol 3-kinase. *Mol Cell Biol*. 23:2501-2514.

Wang, T., Z. Ming, W. Xiaochun, and W. Hong. 2011. Rab7: role of its protein interaction cascades in endo-lysosomal traffic. *Cellular signalling*. 23:516-521.

Yamano, K., A.I. Fogel, C. Wang, A.M. van der Bliek, and R.J. Youle. 2014. Mitochondrial Rab GAPs govern autophagosome biogenesis during mitophagy. *eLife*. 3:e01612.

Yan, Y., R.J. Flinn, H. Wu, R.S. Schnur, and J.M. Backer. 2009. hVps15, but not Ca2+/CaM, is required for the activity and regulation of hVps34 in mammalian cells. *Biochem J*. 417:747-755.

Yasuda, S., S. Morishita, A. Fujita, T. Nanao, N. Wada, S. Waguri, G. Schiavo, M. Fukuda, and T. Nakamura. 2016. Mon1-Ccz1 activates Rab7 only on late endosomes and dissociates from the lysosome in mammalian cells. *Journal of cell science*. 129:329-340.

Zerial, M., and H. McBride. 2001. Rab proteins as membrane organizers. *Nat Rev Mol Cell Biol*. 2:107-117.

Zhang, F., Z. Wang, M. Lu, Y. Yonekubo, X. Liang, Y. Zhang, P. Wu, Y. Zhou, S. Grinstein, J.F. Hancock, and G. Du. 2014. Temporal production of the signaling lipid phosphatidic acid by phospholipase D2 determines the output of extracellular signal-regulated kinase signaling in cancer cells. *Mol Cell Biol*. 34:84-95.

Figures

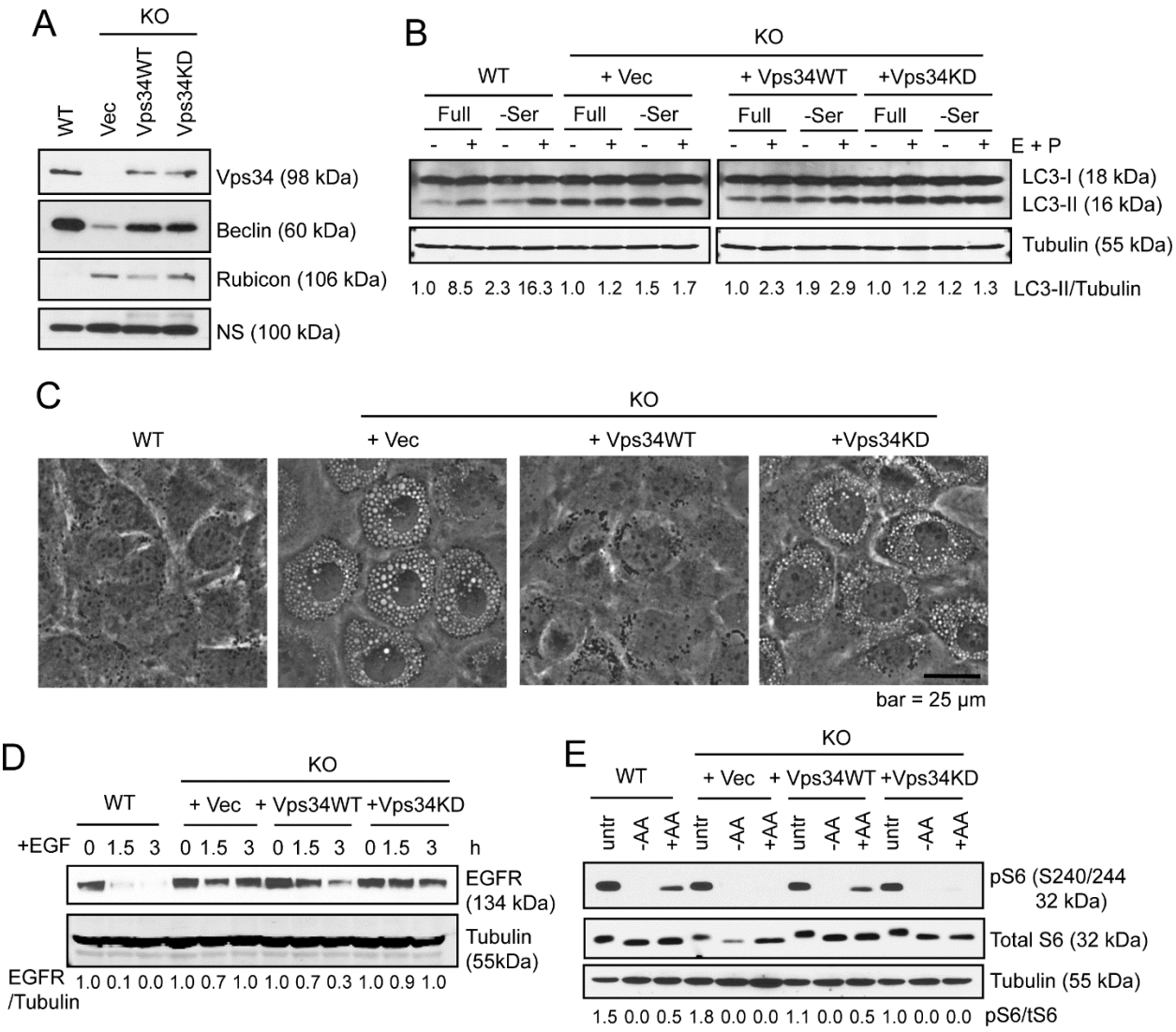

Figure 1. Vps34 functions are dependent on its catalytic activity. (A) Empty vector (Vec), HA-tagged Vps34 wild-type (Vps34WT) or Vps34 kinase-dead mutant K771A (Vps34KD) were stably expressed in Vps34$^{-/-}$ MEFs. Indicated proteins were probed via immunoblotting. NS, non-specific band. (B) Vps34 wild-type but not kinase-dead rescues autophagy flux. Indicated MEFs were cultured in full or serum-free media for 6 h, with or without 10 μg/mL E64D and 10 μg/mL Pepstatin A (E + P) to block lysosomal degradation. Autophagy flux is evaluated by comparing LC3-II/tubulin levels in the presence and absence of the protease inhibitors using ImageJ. (C)

Intracellular vacuolization induced by Vps34 ablation is rescued by wild-type but not kinase-dead Vps34. Indicated cells were photographed and representative images are shown. (n=3) (D) EGFR degradation is rescued by wild-type but not kinase-dead Vps34. Indicated cells were serum-starved overnight and then stimulated with 100 ng/mL EGF for indicated times. The level of EGF receptor was analyzed by immunoblotting. Relative level of EGFR vs tubulin of a representative experiment of two independent experiments is shown. (E) Amino acid-induced mTOR signaling is rescued by wild-type but not kinase-dead Vps34. Indicated cells were left untreated (untr), amino acid starved (-AA), or starved and re-stimulated with 2x amino acids for 30 min (+AA). Cell lysates were probed with indicated antibodies by immunoblotting. The ratio of pS6 vs total S6 of a representative experiment (of two independent experiments) is shown.

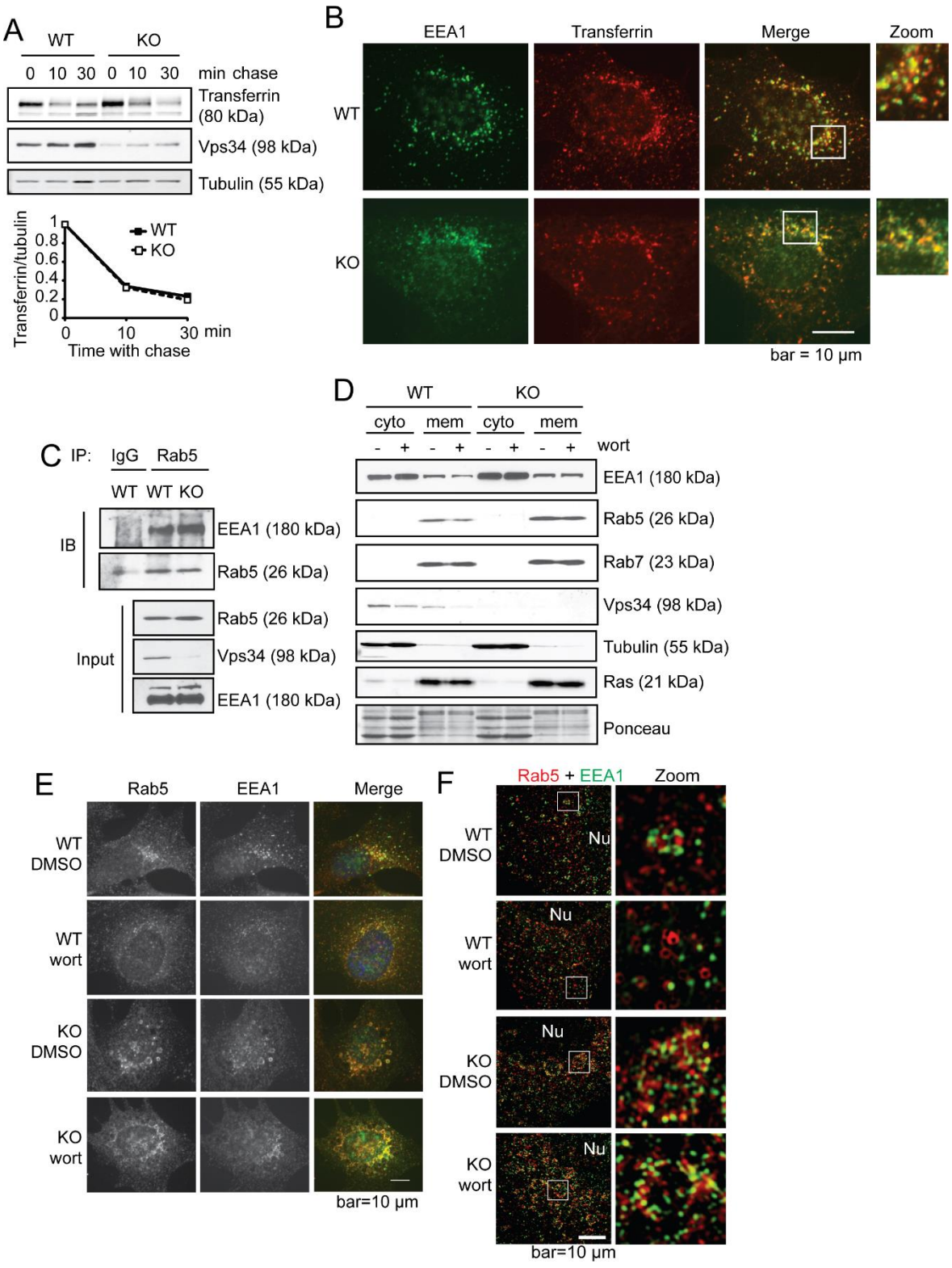

Figure 2. Ablation of Vps34 does not affect early endosome function. (A) Transferrin recycling is unaffected by Vps34 deletion. $Vps34^{+/+}$ or $Vps34^{-/-}$ MEFs were serum starved for 4 h before incubating with biotinylated transferrin. Unbound biotinylated transferrin was stripped, and cells were chased with unlabelled transferrin for the indicated times. The level of intracellular biotinylated-transferrin was analyzed by immunoblotting and quantified by ImageJ. (n=3) (B) EEA1-positive early endosomes in $Vps34^{-/-}$ MEFs can receive transferrin cargo. Cells were loaded with Transferrin-AF-594, fixed, and immunostained for EEA1. Cells were observed under deconvolution microscope. Note that colocalization between EEA1 and transferrin was observed in both $Vps34^{+/+}$ and $Vps34^{-/-}$ cells. (C) Rab5-EEA1 interaction is not disrupted in $Vps34^{-/-}$ cells. $Vps34^{+/+}$ and $Vps34^{-/-}$ MEFs were immunoprecipitated for endogenous Rab5 then probed for EEA1. Note that $Vps34^{-/-}$ cells show anti-Vps34 immune-reactivity due to incomplete adenoviral-Cre infection in the cell population, not an incomplete knockdown in individual cells. (D) EEA1 membrane localization is refractory to wortmannin treatment in $Vps34^{-/-}$ cells. Subcellular fractionation was performed in $Vps34^{+/+}$ and $Vps34^{-/-}$ MEFs in the presence or absence of wortmannin (1 μM). Cytoplasmic (cyto) and membrane (mem) fractions were analyzed by immunoblotting. Note that wortmannin treatment leads to decreased EEA1 membrane localization in $Vps34^{+/+}$ but not in $Vps34^{-/-}$ cells. (E and F) Rab5 and EEAl colocalize on enlarged early endosomes in $Vps34^{-/-}$ MEFs. $Vps34^{+/+}$ and $Vps34^{-/-}$ MEFs were treated with DMSO or wortmannin (1 μM, wort) for 1 h. Cells were immunostained for endogenous Rab5 and EEA1, counterstained with DAPI, and observed under deconvolution microscope. (n=4) (E) or with a super resolution Structured Illumination Microscope (SIM) (F). Note that two signals will not be observed to completely overlap under super resolution microscopy, and colocalization is considered when two signals are in close proximity. White arrows point to early endosomes, and enlarged late endosomes are outlined in (F). The boxed areas are further zoomed in. Nu: nucleus. Note that in wild-type cells, Rab5 and EEA1 colocalize on endosomes, while wortmannin treatment disrupts the punctate staining pattern and Rab5-EEA1 colocalization. In $Vps34^{-/-}$ cells, Rab5 and EEA1 colocalize on enlarged endosomes and the colocalization is not affected by wortmannin.

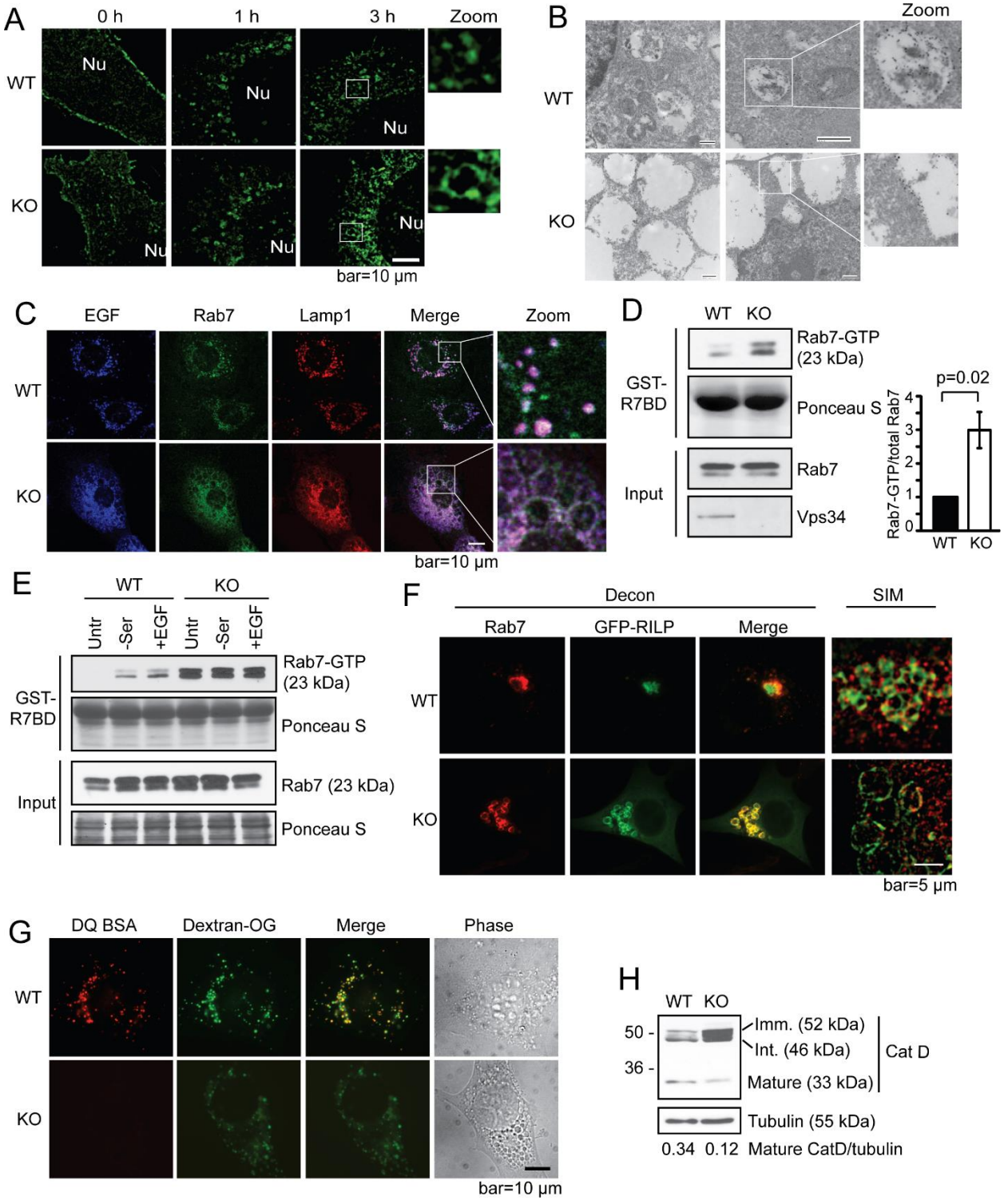

Figure 3. Ablation of Vps34 leads to Rab7 hyperactivation, late endosome enlargement, and defective lysosomal function. (A) Internalized EGFR localizes to the limiting membrane of enlarged endosomes in Vps34$^{-/-}$ cells. GFP-EGFR was expressed in Vps34$^{+/+}$ and Vps34$^{-/-}$ MEFs. Cells were serum starved and stimulated with 100 ng/mL EGF for the indicated times. The GFP-EGFR localization was analyzed by super resolution SIM. The boxed areas are further zoomed in. Nu: nucleus. (n=4) (B) GFP-EGFR were transfected into Vps34$^{+/+}$ or Vps34$^{-/-}$ MEFs. Cell were starved overnight, then left untreated or stimulated with 100 ng/mL EGF in serum-free media for 1.5 h. Immuno-gold EM against anti-GFP reveals the accumulation of GFP-EGFR in the lumen of endosomes in Vps34$^{+/+}$ but on the limiting membrane of enlarged endosomes in Vps34$^{-/-}$ cells. Two representative cells of each cell type are shown. The boxed areas are further zoomed to help visualize gold particles. (C) EGF accumulates on the limiting membrane of enlarged late endosomes in Vps34$^{-/-}$ cells. Vps34$^{+/+}$ and Vps34$^{-/-}$ MEFs were stimulated with EGF-AF-647 for 45 min. Cells were stained for endogenous Rab7 and Lamp1, and analyzed by confocal microscopy. (D) Rab7-GTP levels are increased in Vps34$^{-/-}$ MEFs. Rab7 activity assay was performed using the Rab7 binding domain (R7BD) of RILP fused to GST, which pulls down GTP-bound Rab7. Shown on the right is the relative amount of Rab7-GTP averaged from three independent experiments. (E) Vps34$^{-/-}$ cells have elevated Rab7-GTP level that is refractory to starvation and EGF stimulation. Vps34$^{+/+}$ and Vps34$^{-/-}$ MEFs were left untreated (untr), or serum starved (-ser), or starved plus 100 ng/mL EGF stimulation (+EGF). Rab7 activity assay was performed using GST-R7BD. (F) Rab7 effector RILP localizes on the limiting membrane of enlarged late endosomes in Vps34$^{-/-}$ cells. GFP-RILP was transfected in Vps34$^{+/+}$ and Vps34$^{-/-}$ cells. Cells were fixed and immunostained for endogenous Rab7. Cells were observed under deconvolution or SIM microscopes. Note that RILP overexpression causes perinuclear clustering of late endosomes in wild-type cells, as expected, and that Rab7 and RILP colocalize on enlarged late endosome structures. (G) Lysosomal protease activity is diminished in Vps34$^{-/-}$ MEFs. Cells were loaded with 10 μg/mL Dextran-Oregon Green for 16 h plus 4 h chase, then loaded with DQ-BSA for 1 h. Cells were washed extensively and the fluorescence pattern was analyzed in live cells using deconvolution microscope. Note that DQ-BSA cleavage is severely compromised in Vps34$^{-/-}$ cells. (n=3) (H) Vps34 deletion disrupts cathepsin D maturation. The steady-state levels of immature (52 kDa), intermediate (46 kDa), and mature (33 kDa) cathepsin D were analyzed by immunoblotting. (n=4)

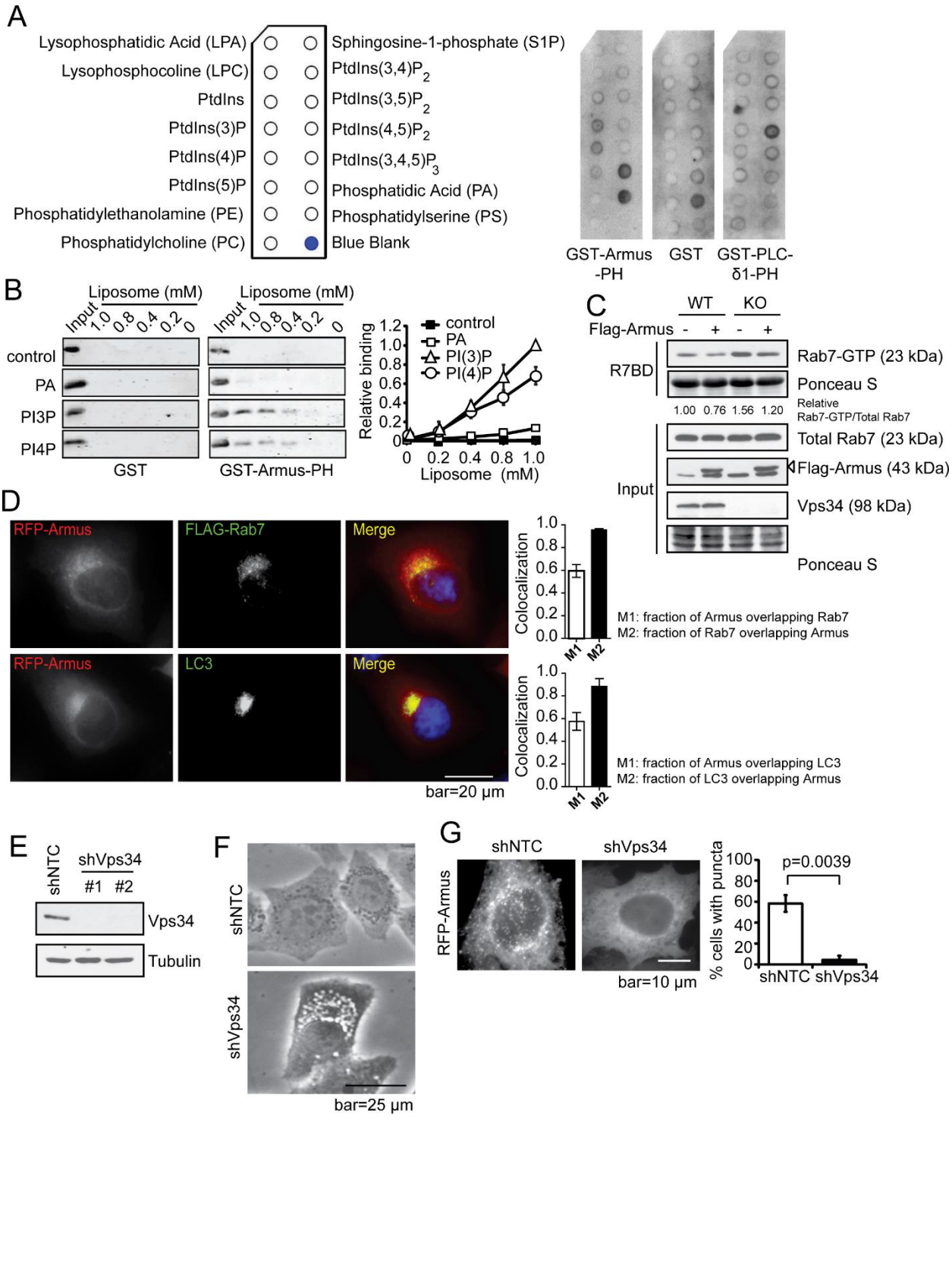

Figure 4. Vps34 controls the recruitment of Rab7 GAP Armus to endosomes. (A) Armus is a PI(3)P-binding protein. 0.5 μg/ml of Armus-PH-GST, GST only, or PLC-δ1-PH-GST was added to PIP strips and detected by anti-GST antibody. PLC-δ1-PH-GST binding to $PI(4,5)P_2$ was used as a positive control. Shown is the result of one of the two independent experiments. (B) The binding between the purified recombinant protein GST or GST-ArmusPH domain and liposomes containing different phospholipids was detected by immunoblotting using an anti-GST antibody. The control liposomes are composed of PC and PE. PA, PI(3)P, and PI(4)P liposomes are composed of PC, PE, plus PA, PI(3)P, or PI(4)P, respectively. Quantitation of the ArmusPH lipid binding results is shown on the right. Relative binding of GST-ArmusPH to various liposomes were normalized by the amount of input protein. The results shown are from three independent experiments. (C) Armus expression reduces the increased Rab7-GTP levels in $Vps34^{-/-}$ cells. Flag- or Myc-Armus (547-928) was expressed in $Vps34^{+/+}$ and $Vps34^{-/-}$ MEFs, then a Rab7 activity assay was performed. Note that Armus expression leads to reduced Rab7-GTP in both $Vps34^{+/+}$ and $Vps34^{-/-}$ cells. Relative amount of Rab7-GTP vs total Rab7 was determined by Image J and is expressed as the ratio to that of the control wild-type cells. The shown immunoblot is a representative of four independent experiments. (D) HeLa cells were transiently transfected with RFP-Armus and Flag-Rab7. Immunofluorescence was performed using RFP, anti-Flag (green), or anti-LC3 (endogenous) antibodies. DAPI was used to visualize the nucleus. Note that overexpressed Rab7 co-localizes with overexpressed Armus and endogenous LC3. Manders coefficient was calculated from 4 cells of each sample. M1 indicates the fraction of protein A overlapping with protein B, and M2 indicates the fraction of protein B overlapping with protein A. (E) HeLa cells were lentivirally infected with non-targeting control shRNA (shNTC) or two independent Vps34 shRNAs (shVps34), and analyzed for Vps34 protein level by immunoblotting. (n=3) (F) Cell morphology of HeLa cells expressing Vps34 shRNA was observed by phase contrast microscopy. Note that Vps34 silencing leads to vacuolization. (n=3) (G) Vps34 silencing ablates punctate Armus localization. RFP-Armus was expressed in shNTC or shVps34-expressing HeLa cells. Cells were observed under fluorescence microscope. Note the punctate pattern of Armus in the control cells but the diffused pattern in shVps34 cells. The average numbers of cells with punctate RFP-Armus localization were obtained by 3 blind countings of 100 cells each, and are shown on the right.

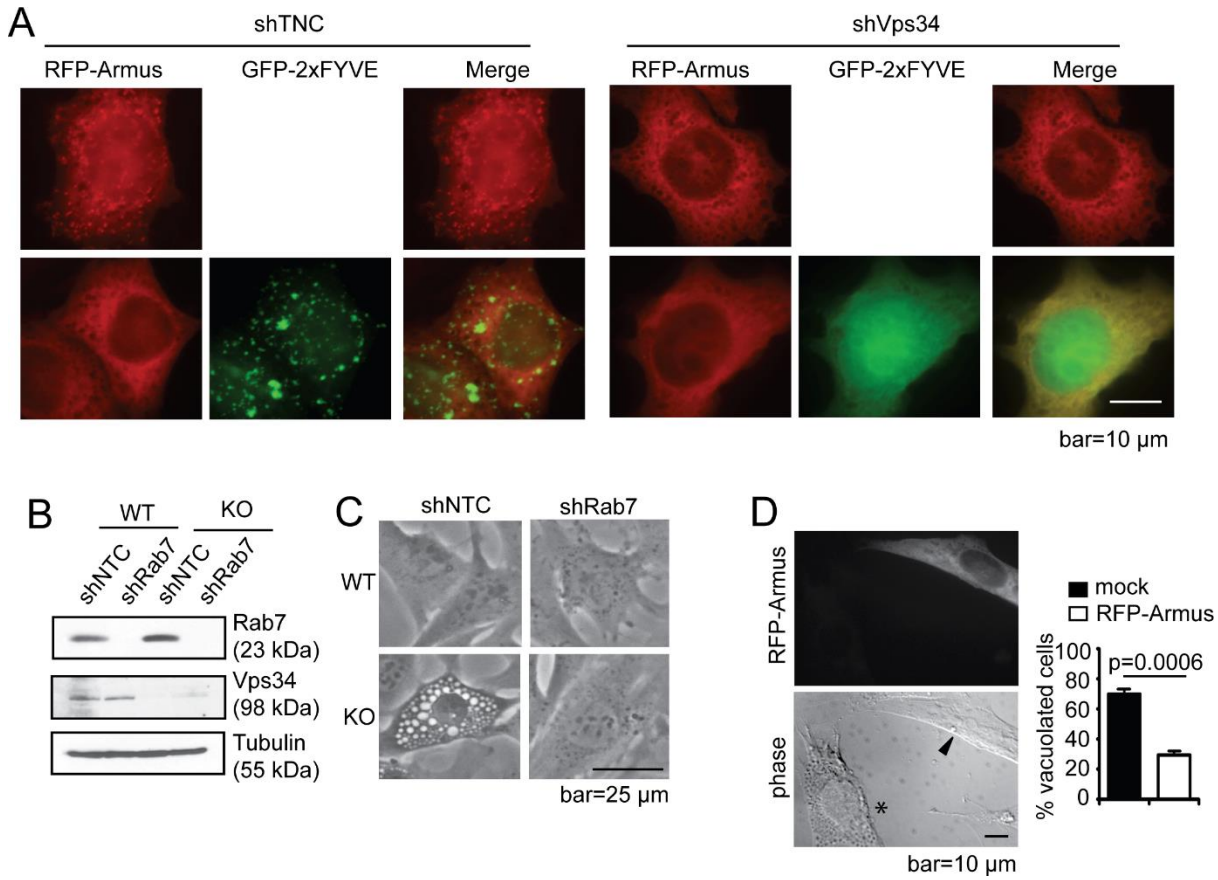

Figure 5. Inhibition of Rab7 or Armus expression leads to the disappearance of intracellular vacuoles. (A) GFP-2xFYVE and RFP-Armus were expressed in shNTC or shVps34 expressing HeLa cells. Cells were observed under deconvolution microscope. Some large GFP-2xFYVE aggregates are observed in shNTC cells, which is common with GFP-2xFYVE overexpression. Note that expression of GFP-2xFYVE leads to the loss of punctate Armus localization in shNTC cells, and that both GFP-2xFYVE and RFP-Armus show a diffused pattern in shVps34 cells. (n=3) (B and C) Non-targeting (shNTC) and Rab7 shRNA were lentivirally expressed in Vps34$^{+/+}$ and Vps34$^{-/-}$ MEFs. (B) Cell lysates were probed for indicated proteins. (C) Cell morphology was observed under phase-contrast microscope. Note that Rab7 knockdown prevents vacuolization in Vps34$^{-/-}$ cells. (n=3) (D) Full-length RFP-Armus was expressed in Vps34$^{-/-}$ MEFs. Cells were observed under deconvolution microscope. Asterisk denotes vacuolated cell, arrowhead points to transfected cell. Cells with more than 10 enlarged vacuoles were quantified in mock or RFP-

Armus transfected cells. Shown is the average of 3 blind countings of over 100 cells. Note that Armus-expressing cells display reduced vacuolization.

Supplementary Figure

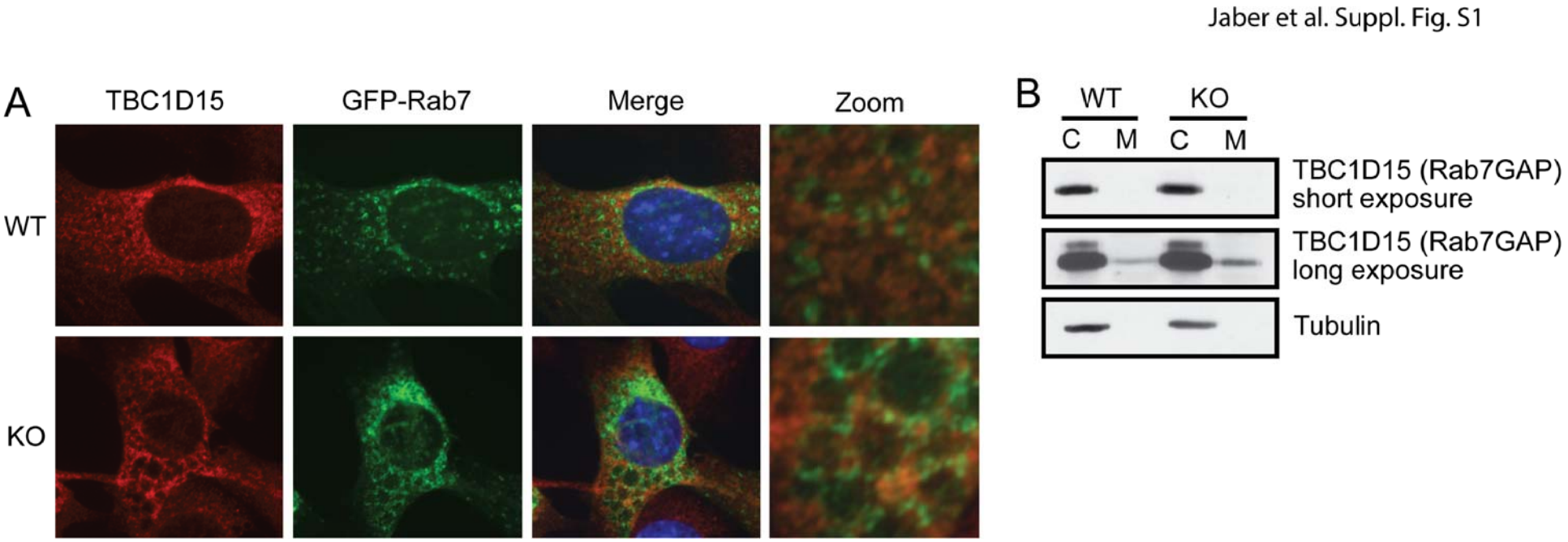

Fig. S1. Vps34 deletion has little effect on TBC1D15 localization. (A) GFP-Rab7 was transfected in Vps34$^{+/+}$ and Vps34$^{-/-}$ cells. Cells were fixed and immunostained for endogenous TBC1D15. Cells were observed under deconvolution microscope. Note that there is no obvious difference in the localization of TBC1D15 between Vps34$^{+/+}$ and Vps34$^{-/-}$ cells. (B) Vps34 deletion has minimal effect on TBC1D15 membrane localization. Subcellular fractionation was performed in Vps34$^{+/+}$ and Vps34$^{-/-}$ MEFs. Cytoplasmic (cyto) and membrane (mem) fractions were analyzed by immunoblotting. Note that there is only a slight increase in membrane localization of endogenous TBC1D15 in Vps34$^{-/-}$ MEFs.

Supplementary Figure

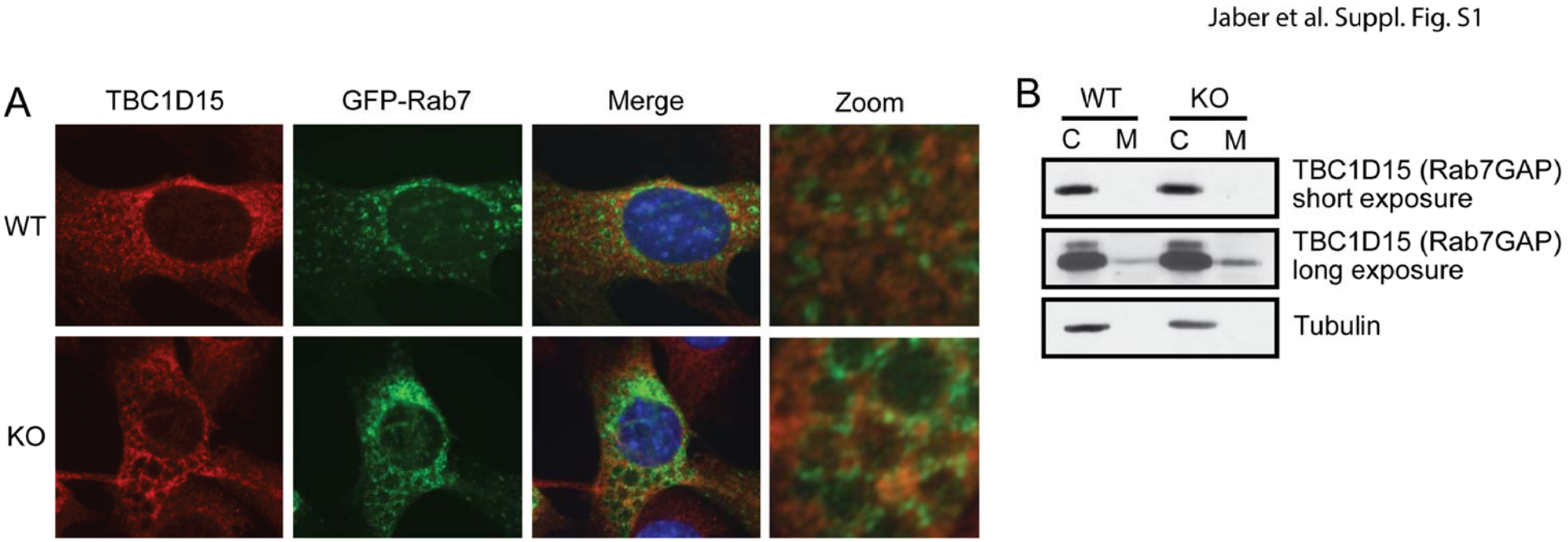

Fig. S1. Vps34 deletion has little effect on TBC1D15 localization. (A) GFP-Rab7 was transfected in Vps34$^{+/+}$ and Vps34$^{-/-}$ cells. Cells were fixed and immunostained for endogenous TBC1D15. Cells were observed under deconvolution microscope. Note that there is no obvious difference in the localization of TBC1D15 between Vps34$^{+/+}$ and Vps34$^{-/-}$ cells. (B) Vps34 deletion has minimal effect on TBC1D15 membrane localization. Subcellular fractionation was performed in Vps34$^{+/+}$ and Vps34$^{-/-}$ MEFs. Cytoplasmic (cyto) and membrane (mem) fractions were analyzed by immunoblotting. Note that there is only a slight increase in membrane localization of endogenous TBC1D15 in Vps34$^{-/-}$ MEFs.